J. Astrophys. Astr. (2006) **27,** 399–409

Chemistry of Carbon Rich Star IRAS 15194–5115

A. Ali
King Abdulaziz University, Faculty of Science, Astronomy Department, P.O. Box 80 203, Jeddah 21589, Saudi Arabia.
Permanent address: Cairo University, Faculty of Science, Astronomy Department, Giza, Egypt.

Received 2004 December 28; accepted 2006 November 7

Abstract. We have constructed two gas-phase models to study the chemistry of circumstellar envelope surrounding the carbon-rich variable star IRAS 15194–5115. The network used consists of 3893 reactions involving 397 gas-phase species. The derived fractional abundances for many molecules are in excellent agreement with values obtained from observations. The predicted column densities from the two models go well with the observed values of carbon star IRC + 10216. The dominant formation routes for three groups of species are discussed through the inner and outer envelopes.

Key words. Molecular data—molecular processes—stars: AGB—stars: individual: IRAS 15194–5115.

1. Introduction

IRAS 15194–5115 is the third brightest carbon star at 12 μm and the brightest one known in the southern hemisphere. The object was identified as a carbon star from optical and infrared spectroscopy (Meadows *et al.* 1987), and from its position in the [K-L, 12 μm–12 μm] color–color diagram (Epchtein *et al.* 1987). Le Berte & Epchtein (1990) have monitored the star in the near-infrared and derived a period of 578 days. Feast *et al.* (2003) presented JHKL observations for this star extending over about 18 years. Based on their data, the pulsation period of IRAS 15194–5115 is 575 days and has remained essentially constant over this time span. Their results suggest that there are obscuration changes due to the formation of dust clouds of limited extent in the line of sight. From the radio and far-infrared observations given by Ryde *et al.* (1999), they suggest that the object appears to be a highly evolved AGB-star, but the carbon star properties combined with inferred low $^{12}C/^{13}C$ ratio make the evolutionary status of this star uncertain. It may have been a J-star for which the $^{12}C/^{13}C$ ratio has remained low, or it may be a star of 5 to 8 solar masses, which has recently become a carbon star due to the quenching of hot bottom burning.

IRAS 15194–5115 in the infrared region shows similarities to the well-studied carbon star IRC + 10216. However, the mass-loss rate of IRAS 15194–5115 is higher than the average carbon stars. Schoier & Olofsson (2001) measured a median mass-loss rate for carbon stars of $\sim 3 \times 10^{-7}\,M_{\odot}/yr$. As reported by Woods *et al.* (2003,

hereafter WSNO), this suggests that IRAS 15194–5115 is going through the superwind phase evolution at the end of the AGB, and will soon eject its entire stellar mantle. Nyman *et al.* (1993, hereafter NOJBCW) have used radio observations to study the molecular species of IRAS 15194–5115 and found that circumstellar abundances, except for a few species, are comparable to those in IRC + 10216. The most striking difference between these two objects was the $^{12}C/^{13}C$ ratio, which appears to be at least five times lower in IRAS 15194–5115. A millimeter molecular line survey for IRAS 15194–5115 and six other high mass-loss carbon stars have been presented by WSNO. Their reported abundances for 24 molecular species in the seven stars agreed to within a factor of five of each other, indicating that circumstellar envelopes (CSEs) around carbon stars have similar molecular compositions. The derived abundance ratio of IRAS 15194–5115 relative to IRC + 10216 given by WSNO is higher by a factor of ~ 4 as compared with the data presented by NOJBCW. This was explained by WSNO as being due to the difference in mass loss rates of the two stars.

Circumstellar envelopes of carbon-rich stars are very rich in molecular species. More than 50 different molecular species have been observed to date in IRC + 10216. In addition to simple carbon-bearing molecules, large carbon-chain molecules like cyanopolyynes, hydrocarbon radicals, carbenes, and sulphur and silicon bearing species have been detected in its envelope (Guelin *et al.* 1998; Olofsson 1997; Olofsson 1994; Cernicharo *et al.* 1991). These species can be divided into parent and daughter molecules. Parent molecules are formed in thermodynamic equilibrium in the stellar photosphere and are ejected with the outflowing material. When the ejected gas reaches the external layers of the envelope where UV photons can penetrate, parent molecules are dissociated into reactive daughter products that give rise to the outer envelope chemistry (Fuente *et al.* 1998).

Early chemical schemes of carbon rich CSEs based on models of interstellar chemistry were published by Glassgold *et al.* (1986), Nejad & Millar (1987) and Glassgold *et al.* (1987). These types of models are in reasonably good agreement with observations, but they could not explain the generation of the larger molecules. Recently, several new models have been proposed for predicting the larger molecules for the brightest carbon rich star IRC + 10216. Millar *et al.* (2000), developed a new chemical model of the outer CSE of IRC + 10216 in which carbon-bearing molecules up to 23 carbon atoms were included. This work was an extension of the earlier work of Bettens & Herbst (1995). In their new model, they extended standard models of gas-phase interstellar chemistry to produce unsaturated molecules as large as fullerenes. The chemical network used in the previous model have been used to model the enhanced density shells around IRC + 10216 (Brown & Millar 2003) and the synthesis of benzene in the protoplanetary nebula (PPN) CRL618 (Woods *et al.* 2002).

Since the chemistry of IRAS 15194–5115 did not study theoretically up till now, the goal of the present paper is to study the chemistry of this object. For this purpose, we have developed two gas-phase models. The first model (model 1) is constructed to compare with the observations reported by NOJBCW, while the second model (model 2) is to compare with the recent observations of WSNO. The purpose of these two models is to predict the fractional abundance and some physical parameters observed for this object. In section 2, we present the initial parameters of the two models, equations used to calculate gas density, temperature and visual extinction and chemical network

Table 1. Initial parameters for models 1 and 2.

	Model 1	Model 2
Mass loss rate	$5 \times 10^{-5}\,M_{\odot}$/yr (NOJBCW)	$1 \times 10^{-5}\,M_{\odot}$/yr (WSNO)
Expansion velocity	22 km/s (NOJBCW)	21.5 km/s (WSNO)
Initial radius	5×10^{15} cm	
Final radius	5×10^{17} cm	
UV radiation	Standard interstellar value	
Ionization rate (ζ)	Standard interstellar value	
H_2	See equation (1)	
C/O	1.19	

database. In section 3, we show the results of the two models and discuss the chemistry of several species in inner and outer parts of the envelope. Conclusions are given in section 4.

2. Physical models

For this study, we have assumed that the gas in IRAS 15194–5115 expands in a spherically symmetric outflow with constant velocity. We have adopted the expansion velocity and mass-loss rate of (NOJBCW) for model 1 and (WSNO) for model 2 (see Table 1). The gas density of H_2 is estimated as

$$n_{H_2}(r) = \frac{\dot{M}}{4\pi r^2 v_e m_H}, \tag{1}$$

where $\dot{M}$ is the stellar mass loss rate, v_e is the expansion velocity, r is the distance from the star and m_H is the mass of molecular hydrogen (Willacy & Millar 1997). The temperature is given as a function of the shell radius according to the following temperature profile

$$T(r) = \max\left[100\left(\frac{r}{r_i}\right)^{-0.79}, 10\right], \tag{2}$$

where r_i is the initial radius of the shell (Millar & Herbst 1994). The visual extinction, A_v, is estimated according to the relation

$$\frac{N_{H_2}}{A_v} = 10^{21}\,\mathrm{cm}^{-2}\,\mathrm{mag}^{-1}, \tag{3}$$

where the column density of H_2 is given by

$$N_{H_2} = n_{H_2}(r) r. \tag{4}$$

Table 2. Adopted initial fractional abundances of parent species with respect to $n(H_2)$.

Species	Initial fractional abundance
He	0.15
CO	6.0E − 4
N_2	2.0E − 4
C_2H_2	2.0E − 5
HCN	1.0E − 5
CS	1.0E − 6
CH_4	2.0E − 6
H_2S	1.0E − 6
SiH_4	4.0E − 6
SiS	3.0E − 7

The calculations of the radial distribution of molecular abundances start at a radius of 5×10^{15} cm, until the outer radius of 5×10^{17} cm. According to equation (2), the temperature varies from ~ 100 K at the inner radius to 10 K at the outer radius in both models. Most of the predicted species give their peak values between 9×10^{15} cm and 9×10^{16} cm, where the temperature varies from $\sim$ 60 to 10 K. This range of temperature roughly agrees with the observed kinetic temperature range of $\sim$ 30 to 10 K given by WSNO and that given in Fig. 4 of Ryde *et al.* (1999). With respect to the density derived from equation (1) in the range 9×10^{15} cm to 9×10^{16} cm, models 1 and 2 give density range of $\sim 8.0 \times 10^4$ to 8×10^2 cm^{-2} and $\sim 5.0 \times 10^5$ to 5×10^3 cm^{-2} respectively. These values are compatible with the observed density range $\sim 10^5$ to 10^2 cm^{-2}, given by WSNO.

Initial parameters like mass loss, expansion velocity, UV radiation and cosmic ray ionization rate are given in Table 1 for our two models. Initial fractional abundances of parent species with respect to $n(H_2)$ are given in Table 2. These values are typical of carbon-rich AGB stars. We take into account the effect of self-shielding for H_2 and CO molecules against the photo-dissociation. We have used the chemical reaction network and rate coefficients (RATE 95 data base) of Millar *et al.* (1997). The chemical network has 3893 gas-phase reactions and 397 species.

3. Results and discussion

3.1 *Comparison between observations and calculations*

The results of model 1 show excellent agreement with the observation given by NOJBCW. Table 3 displays a comparison between calculated and observed fractional abundances. The calculated abundances of all species, except for C_3N and C_4H, are in the same order of magnitude as the observed values. The ratios between calculated

Table 3. A comparison between calculated (model 1) and observed (Nyman *et al.* 1993) fractional abundances of IRAS 15194–5115.

Species	NOJBCW	Model 1
CN	1.70E − 06	1.90E − 06
CS	1.20E − 06	1.00E − 06
SiO	4.80E − 07	3.00E − 07
SiS	9.70E − 07	9.80E − 07
HCN	1.00E − 05	9.90E − 06
HNC	9.50E − 08	5.40E − 08
SiC_2	9.00E − 07	4.00E − 07
C_2H	1.60E − 05	1.60E − 05
C_3H	3.60E − 08	3.70E − 08
C_4H	7.40E − 06	1.30E − 07
C_3H_2	9.60E − 08	4.80E − 08
C_3N	1.70E − 07	7.10E − 10
HC_3N	6.40E − 07	2.50E − 07

and observed abundances for most species vary from ~ 0.4 to 1, while abundances for C_3N and C_4H are two orders less than the observed ones.

The results of model 2 are compared with the recent observations given by WSNO. The results given in Table 4, agree well with the observations. The predicted fractional abundances agree within 1–2 orders of magnitude with the observed values. CN, CS, SiO, SiS, HCN, HNC, C_2H, C_3H, C_3H_2 and HC_3N indicate good agreement with similar observed species. The ratios between calculated and observed values for the previous species vary from 0.1 to 1. The observed species C_3N, HC_5N, C_2S, C_3S and CH_3CN are given as the upper limit, therefore our results of these species could possibly be reasonable. SiC_2 and C_4H the only two species show less agreement with observations. Their abundances are up to two orders of magnitude less than the observations. In general, the obtained predictions using model 1 match more closely the observations than model 2.

Table 5 shows good agreement between the column densities derived from our two models and the observations of IRC + 10216. We compared our results with that of IRC + 10216, because there are no observed column densities published for the species of IRAS 15194–5115. The first column of Table 5 is the observed column densities given by WSNO, while the second column shows the observations collected from other sources. The calculated column densities for most species given in Table 5 fit well with the observed ones, except for the following species: C_2H which is one order of magnitude larger than the observed values, C_3N is about one order less than the observed value and the large molecules HC_5N, HC_7N and HC_9N are 1–3 orders less than the observed values. The large value of C_2H in our object comparing with IRC + 10216, could be due to the observed fractional abundance of this

Table 4. A comparison between calculated (model 2) and observed (Woods *et al.* 2003) fractional abundances of IRAS 15194–5115.

Species	WSNO	Model 2
CN	1.20E − 06	2.50E − 06
CS	2.00E − 06	9.90E − 07
SiO	1.70E − 06	3.00E − 07
SiS	4.60E − 06	1.00E − 06
HCN	*1.20E − 05	9.90E − 06
HNC	3.30E − 07	4.90E − 08
SiC_2	8.10E − 06	5.60E − 07
C_2H	1.50E − 05	2.00E − 05
C_3H	9.20E − 08	6.90E − 08
C_4H	2.80E − 05	8.20E − 07
C_3H_2	6.00E − 07	3.40E − 07
C_3N	< 4.80E − 07	6.70E − 09
HC_3N	2.10E − 06	4.90E − 07
HC_5N	< 4.50E − 06	1.50E − 08
C_2S	< 3.00E − 08	4.20E − 09
C_3S	< 7.20E − 08	4.80E − 09
CH_3CN	< 1.20E − 06	1.30E − 09

*HCN = 5.5 × $H^{13}CN$.

molecule in our object which is about 5 times that of IRC + 10216 (see Table 9 of WSNO).

Bachiller *et al.* (1997, Fig. 5) reported that the abundances of CN, HNC and HCO^+ increase dramatically when the star transits from the stage of AGB, through the proto-PN and PN phases. CN/HCN ratio has a wide varying range from 0.07–0.68 for high mass-loss AGB stars (WSNO), while it has very narrow range ∼ 0.65–0.7 in low mass-loss stars (Olofsson *et al.* 1993). Our derived ratio of CN/HCN from both models fit well with the observations of NOJBCW and WSNO. The observed values of CN/HCN given by WSNO and NOJBCW or our derived values from models 1 and 2 indicate that IRAS 15194–5115 is an early type carbon star (Table 6). Our predicted HNC/HCN ratio also fits well with the observations of NOJBCW and Omont (1993). This value increases by two orders of magnitude in PN phase as compared to CSE. The molecular ion HCO^+ has not been observed in our object, but its derived column density given in Table 5 fits well with the observed values of IRC + 10216. As given in Table 6, the ratio of HCO^+ relative to HCN matches the observed value given by Omont (1993). The previous three ratios, in addition to the $^{12}CO/^{13}CO$ ratio, can be used to estimate the evolutionary status of carbon stars. As the star evolves along AGB, the ratio $^{12}CO/^{13}CO$, which depends on stellar mass, is expected to increase gradually from an initial low value of ∼10–15 (Abia *et al.* 2001).

Table 5. A comparison between observed (IRC + 10216) and calculated (IRAS 15194–5115) column densities (cm^{-2}).

	Observations		Predictions	
Species	WSNO	Other sources	Model 1	Model 2
CN	8.3E + 14		2.74E + 15	1.22E + 15
CS			7.80E + 15	1.93E + 15
HCN			7.72E + 16	1.93E + 16
HNC	2.0E + 13		7.78E + 13	2.38E + 13
SiO			2.34E + 15	5.85E + 14
SiS			7.64E + 15	1.46E + 15
SiC_2			7.92E + 13	1.62E + 14
C_2H	8.9E + 14	3 − 5E + 15(1, 2, 3)	2.30E + 16	3.24E + 16
C_3H	2.1E + 13	3E + 13(1, 4)	5.33E + 13	1.12E + 14
C_4H	9.3E + 14	2 − 9E + 15(1, 3, 4, 5)	1.87E + 14	1.20E + 15
C_5H		2 − 50E13(1, 4)	1.58E + 13	5.54E + 13
C_6H		3 − 30E13(1, 4)	3.89E + 12	2.95E + 13
C_3H_2	1.2E + 13	2E + 13(4)	3.53E + 13	1.65E + 14
C_3N	2.0E + 14	2 − 4E14(4, 6)	4.93E + 11	3.26E + 12
C_5N		3E + 12(6)	1.58E + 13	1.58E + 12
HC_3N	9.1E + 14	1 − 2E15(4, 6)	4.95E + 14	7.15E + 14
HC_5N	5.8E + 15	2 − 3E14(4, 6)	7.78E + 12	2.19E + 13
HC_7N		1E14(4)	6.12E + 10	3.82E + 11
HC_9N		3E + 13(4)	1.73E + 09	1.15E + 10
HCO^+		3E + 12(7)	1.28E + 13	1.66E + 12
CH_3CN	9.9E + 12	6E + 12(8)	3.60E + 12	9.36E + 11

References: (1) Guelin *et al.* (1997); (2) Groesbeck *et al.* (1994); (3) Avery *et al.* (1992); (4) Kawaguchi *et al.* (1995); (5) Dayal & Bieging (1993); (6) Guelin *et al.* (1998); (7) Olofsson (1997); (8) Guelin & Cernicharo (1991).

Table 6. A comparison between observed and calculated ratios of CN, HNC and HCO^+ relative to HCN.

	NOJBCW	WSNO	Omont 1993	Model 1	Model 2
CN/HCN	0.17	0.1	0.075	0.19	0.25
HNC/HCN	9.5E − 03	2.7E − 02	4.0E − 3	5.5E − 03	4.9E − 03
HCO^+/HCN	–	–	< 2.0E − 4	8.9E − 4	2.3E − 4

3.2 *Molecular formation*

The chemistry through the circumstellar envelope was thought to be consisting of three stages: the inner chemistry, where the parent molecules begin to dissociate; the middle chemistry, where the daughter molecules reach their peak abundances and the

outer chemistry, where interstellar photons dissociate all molecules (Willacy & Millar 1997). Shock waves were thought to affect the dynamics and chemistry of the inner layers of CSE (Kerschbaum & Olofsson 2001). A dynamical and chemical model was established for the inner wind of carbon-rich star IRC + 10216 by Willacy & Cherchneff (1998). This model takes the effect of pulsation-driven shocks on the gas envelope close to the stellar photosphere.

3.2.1 *CN, HCN and HNC species*

CN is the daughter product of the parent molecule HCN. Its formation occurs due to the photo-dissociation of HCN only in the inner envelope and both HCN and HNC in the outer envelopes. The parent molecular ion $HCNH^+$ is responsible for the formation of HCN and HNC via dissociative recombination with electrons in the inner and outer envelopes. The main formation routes of CN, HCN and HNC in the inner part are initiated by reactions involving H_3^+.

$$H_3^+ \xrightarrow{CO} HCO^+ \xrightarrow{HCN} HCNH^+ \xrightarrow{e} HCN \xrightarrow{h\nu} CN. \tag{5}$$

$$H_3^+ \xrightarrow{CO} HCO^+ \xrightarrow{HCN} HCNH^+ \xrightarrow{e} HCN. \tag{6}$$

In the outer envelope the dominant formation routes for the previous three species are initiated by carbon ion C^+

$$C^+ \xrightarrow{NH} CN^+ \xrightarrow{H_2} HCN^+ \xrightarrow{H_2} HCNH^+ \xrightarrow{e} HNC \xrightarrow{h\nu} CN. \tag{7}$$

$$C^+ \xrightarrow{NH} CN^+ \xrightarrow{H_2} HCN^+ \xrightarrow{H_2} HCNH^+ \xrightarrow{e} HCN. \tag{8}$$

CN radial abundance distribution shows an increase and then a gradual decrease through a peak at 2×10^{16} cm (Fig. 1). HNC has the same behaviour as CN, except that its peak is at 3×10^{16} cm.

3.2.2 *Organo–nitrogen species*

The main route that produces cyanopolyynes in the inner envelope occur via reactions between CN and $C_{2n}H_2$, where $n = 1, 2, 3$ and 4,

$$CN \xrightarrow{C_{2n}H_2} HC_{2n+1}N. \tag{9}$$

In the outer region, the following main routes are responsible for the formation of cyanopolyynes series:

$$C_3^+ \xrightarrow{H_2} C_3H^+ \xrightarrow{H_2} C_3H_3^+ \xrightarrow{N} H_2C_3N^+ \xrightarrow{e} HC_3N. \tag{10}$$

$$C_5^+ \xrightarrow{H_2} C_5H^+ \xrightarrow{N} C_5N^+ \xrightarrow{H_2} HC_5N^+ \xrightarrow{H_2} H_2C_5N^+ \xrightarrow{e} HC_5N. \tag{11}$$

$$CN \xrightarrow{C_6H_2} HC_7N. \tag{12}$$

$$CN \xrightarrow{C_8H_2} HC_9N. \tag{13}$$

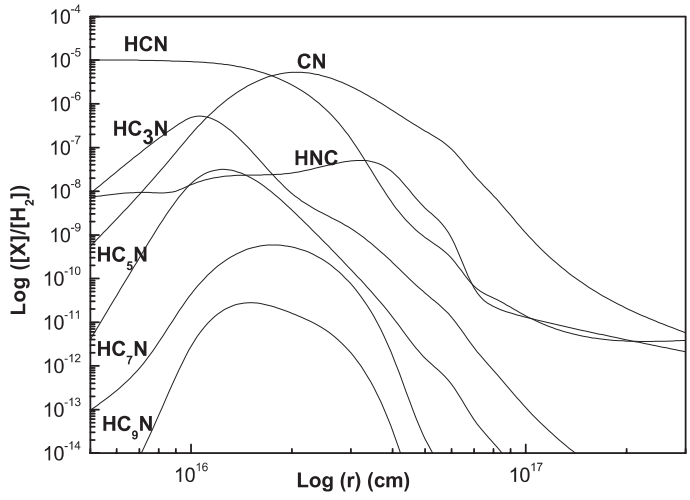

Figure 1. The radial distribution of CN, HNC and organo-nitrogen species (model 2).

Figure 1 shows the radial distribution of the fractional abundances for organo-nitrogen species HCN, HC_3N, HC_5N, HC_7N and HC_9N. HC_3N and HC_5N molecules peak at about 1×10^{16} cm, while HC_7N and HC_9N molecules roughly peak at 2×10^{16} cm.

3.2.3 *Hydrocarbon species*

The formation of hydrocarbon species C_2H, C_3H, C_4H, C_5H and C_6H in the inner envelope occur according to the following routes:

$$C_2H_2 \xrightarrow{h\nu} C_2H. \tag{14}$$

$$C_2H_2 \xrightarrow{h\nu} C_2H_2^+ \xrightarrow{H_2} C_2H_4^+ \xrightarrow{C_2H_2} C_4H_5^+ \xrightarrow{e} C_3H_4 \xrightarrow{h\nu} C_3H_2 \xrightarrow{h\nu} C_3H. \tag{15}$$

$$C_2H \xrightarrow{C_2H_2} C_4H_2 \xrightarrow{h\nu} C_4H. \tag{16}$$

$$C_2H_2 \xrightarrow{h\nu} C_2H_2^+ \xrightarrow{H_2} C_2H_4^+ \xrightarrow{C_2H_2} H_2C_3H^+ \xrightarrow{C_2H_2} C_3H_3^+ \xrightarrow{C_2H_2} C_5H_3^+ \xrightarrow{e} C_5H_2 \xrightarrow{h\nu} C_5H. \tag{17}$$

$$C_2H \xrightarrow{C_2H_2} C_4H_2 \xrightarrow{h\nu} C_4H_2^+ \xrightarrow{C_2H_2} C_6H_4^+ \xrightarrow{e} C_6H. \tag{18}$$

The route schemes 15 and 17 initiated by photo-dissociation of acetylene C_2H_2, followed by ion-neutral reactions, dissociative recombination with electrons and end by photo-dissociation. While route scheme 18 is initiated by neutral–neutral reactions of C_2H_2 with its primary daughter C_2H, followed by ion-neutral reactions and ends

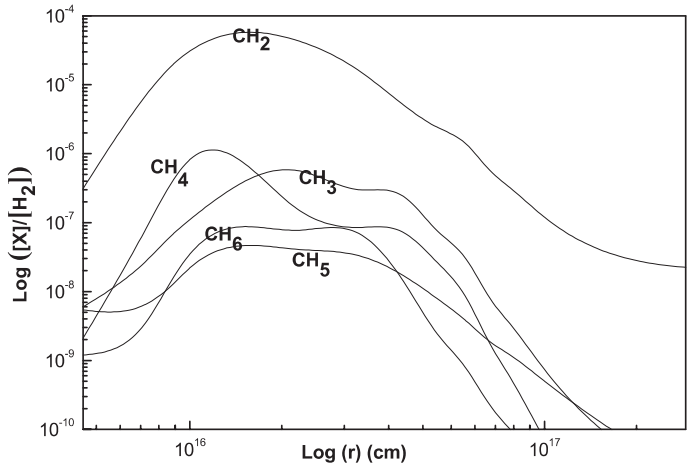

Figure 2. The radial distribution of hydrocarbon species (model 2).

by dissociative recombination with electrons. In the outer envelope, hydrocarbons are formed mainly as follows:

$$C_2H_2 \xrightarrow{h\nu} C_2H. \tag{19}$$

$$C^+ \xrightarrow{C_2H} C_3^+ \xrightarrow{H_2} C_3H^+ \xrightarrow{H_2} C_3H_3^+ \xrightarrow{e} C_3H_2 \xrightarrow{h\nu} C_3H. \tag{20}$$

$$C^+ \xrightarrow{C_3H} C_4^+ \xrightarrow{H_2} C_4H^+ \xrightarrow{H_2} C_4H_2^+ \xrightarrow{e} C_4H. \tag{21}$$

$$C^+ \xrightarrow{C_2H} C_3^+ \xrightarrow{H_2} C_3H^+ \xrightarrow{H_2} C_3H_3^+ \xrightarrow{C_2H} C_5H_3^+ \xrightarrow{e} C_5H_2 \xrightarrow{h\nu} C_5H. \tag{22}$$

$$C^+ \xrightarrow{C_6} C_7^+ \xrightarrow{H_2} C_7H^+ \xrightarrow{e} C_6H. \tag{23}$$

These routes are started by photo-dissociation of C_2H_2 or ion-neutral reactions of C^+, followed by ion-neutral reactions of H_2, dissociative recombination with electrons and photo-dissociation. Figure 2 displays the predicted radial fractional abundances distribution of hydrocarbons. The peak abundance of these species ranges from $\sim 9 \times 10^{15}$–2×10^{16} cm.

4. Conclusion

We have developed two gas-phase chemical models for the carbon star IRAS 15194–5115. These two models represent the first theoretical trial to model the chemistry of this object. The results of the theoretical models predict clearly the observed species in IRAS 15194–5115. The fractional abundances for several species are derived and compared with observed values. The column densities were also derived and compared with those from the observation of carbon star IRC + 10216. The results of both fractional abundances and column densities show very good agreement with the observations, except for very few species. In general, model 1 predicts the observation better than model 2. The ratios of CN/HCN, HNC/HCN and HCO^+/HCN are

in good agreement with observations of carbon rich stars. Finally, we presented the dominant formation routes responsible for producing CN, HNC, organo-nitrogen and hydrocarbon species in the inner and outer layers of the envelope.

References

Abia, C., Busso, M., Gallino, R. *et al.* 2001, *ApJ*, **559**, 1117.
Avery, L. *et al.* 1992, *ApJS*, **83**, 363.
Bachiller, R., Forveille, T., Huggins, P. J., Cox, P. 1997, *A & A*, **324**, 1123.
Bettens, R. P. A., Herbst, E. 1995, *Int. J. Mass Spectrom. Ion Proc.*, **149/150**, 321.
Brown, J. M., Millar, T. J. 2003, *MNRAS*, **339**, 1041.
Cernicharo, J., Gottlieb, C. A., Guelin, M., Killian, T. C., Thaddens, P., Vrtilek, J. M. 1991, *ApJ*, **368**, L43.
Dayal, A., Bieging, J. H. 1993, *ApJ*, **407**, L37.
Epchtein, N., Le Bertre, T., Lepine, J. R. D. *et al.* 1987, *A & AS*, **71**, 39.
Feast, M. W., Witelock, P. A., Marang, F. 2003, *MNRAS*, **346**, 878.
Fuente, A., Cernicharo, J., Omont, A. 1998, *A & A*, **330**, 232.
Glassgold, A. E., Mamon, G. A., Omont, A., Lucas, R. 1987, *A & A*, **180**, 183.
Glassgold, A. E., Lucas, R., Omont, A. 1986, *A & A*, **157**, 35.
Groesbeck, T. D., Philips, T. G., Blake, G. A. 1994, *ApJS*, **94**, 147.
Guelin, M., Cernicharo, J. 1991, *A & A*, **244**, L21.
Guelin, M. *et al.* 1997, *A & A*, **317**, L1.
Guelin, M., Meininger, N., Cernicharo, J. 1998, *A & A*, **335**, L1.
Kawaguchi, K., Kasai, Y., Ishikawa, S., Kaifu, N. 1995, *PASI*, **47**, 853.
Kerschbaum, F., Olofsson, H. 2001, Proc. Symposium "The Promise of the Herschel Space Observatory" 12–15 December 2000, Toledo, Spain Esa SP-460, p. 245, July 2001 (eds) Pilbratt, G. L., Cernicharo, J., Heras, A. M., Prusti, T., Haris, R.
Le Bertre, T., Epchtein, N. 1990, "The Infrared Spectral Region of Stars", Proceedings of the International Colloquium held in Montpellier, France, 16–19 October 1990 (eds) Carlos Jaschek, Andrillat, Y., Cambridge, UK: Cambridge University Press, 1991, p. 398.
Meadows, P. J., Good, A. R., Wolstencroft, R. D. 1987, *MNRAS*, **225**, 43p.
Millar, T. J., Farquhar, P. R. A., Willacy, K. 1997, *A & AS*, **121**, 139.
Millar, T. J., Herbst, E., Bettens, R. P. A. 2000, *MNRAS*, **316**, 195.
Nejad, L. A. M., Millar, T. J. 1987, *A & A*, **183**, 279.
Nyman, L.-A., Olofsson, H., Johansson, L. E. B. *et al.* 1993, *A & A*, **269**, 377.
Olofsson, H. 1994, In: Molecules in the Stellar Environment, (ed.) Jorgensen, U. G., Springer-Berlin, p. 113.
Olofsson, H. 1997, *A & SS*, **251**, 31.
Omont, A. 1993, *J. Chem. Soc. Faraday Trans.*, **89(9)**, 2137.
Ryde, N., Schoier, F. L., Olofsson, H. 1999, *A & A*, **345**, 841.
Schoier, F. L., Olofsson, H. 2001, *A & A*, **368**, 969.
Willacy, K., Cherchneff, I. 1998, *A & A*, **330**, 676.
Willacy, K., Millar, T. J. 1997, *A & A*, **324**, 237.
Woods, P. M., Schöier, F. L., Nyman, L.-Å., Olofsson, H. 2003, *A & A*, **402**, 617.
Woods, P. M., Millar, T. J., Zijlstra, A. A., Herbst, E. 2002, *ApJ*, **574**, L167.